Measurement 94 (2016) 326–332

Contents lists available at ScienceDirect

Measurement

journal homepage: www.elsevier.com/locate/measurement

Soft sensor design for mechanical fault detection in PMSM at variable speed

Erik Etien [a,*], Laurent Rambault [a], Sébastien Cauet [a], Anas Sakout [b]

[a] Laboratory of Informatics and Automatic for the Systems (LIAS), University of Poitiers, 86022 Poitiers, France
[b] LASIE, University of La Rochelle, 17042 La Rochelle, France

ARTICLE INFO

Article history:
Received 1 April 2016
Received in revised form 29 July 2016
Accepted 30 July 2016
Available online 1 August 2016

Keywords:
Soft sensor
Mechanical fault detection
Variable speed
PMSM

ABSTRACT

This paper presents a soft sensor (SS) used to localize mechanical faults in a Permanent Magnet Synchronous Machine (PMSM) at variable speed. The speed contains crucial information about the fault and the characteristic frequencies sought can be amplified by a proper observer design to improve the detection procedure. On the other hand, all the measurements are expressed as a function of estimated position in order to obtain a speed independent signature. An original experimental setup based on a mechanical fault emulator is proposed to validate the simulation results. Simulations and experimental results show that the proposed method is effective to amplify the single fault signatures and calculate fault indicator at variable speed.

1. Introduction

Detection of mechanical faults in electrical machines is a real challenge for many years. Among the studied mechanical defects, bearings [1–3] and gearboxes [4–6] provided numerous recent contributions. Although vibration analysis is the most developed method, the exploitation of electrical currents signatures is increasingly studied [7–9]. It is well known that information about the fault is very poor in currents amplitudes [10]. Then, the research has been directed toward the use of the instantaneous frequency [11–13]. In the case PMSM, electrical frequency is directly linked to the rotational speed. As a consequence, the motor speed appears today as an efficient analysis signal in order to perform fault detection. In addition, the particular case of variable speed operations is a real difficulty because characteristic frequencies become speed dependent [14–17]. A powerful solution consists in synchronizing measurements with the mechanical position [18]. However, the availability of a shaft encoder is crucial to synchronous sampling approaches. An alternative is to use a soft sensor to estimate mechanical parameters as speed or mechanical position [19,20]. In the case of AC motors (induction machines or PMSM), this soft sensor may be designed using adaptive observers [21–23].

In this paper, the design of a soft sensor for fault detection in PMSM at variable speed is addressed. The practical case in which the speed and the motor position are not available is considered. This is for example the case when the motor is controlled by an industrial drive. The soft sensor, based on the motor model, provides in one hand the mechanical speed used as the analysis signal containing fault signatures. It is not used for the motor control. On the other hand, it generates a position estimation used for the synchronization. As a consequence, characteristic frequencies become independent from the motor speed and the analysis is simplified. In Section 2, the fault type studied in this paper is defined. The synchronization procedure is detailed in Section 3. In Section 4, the design is described. Conditions for the observer convergence are defined and an interesting resonance property is highlighted. Experimental results validating the proposed procedure are shown in Section 5.

2. Fault signatures on the rotation speed

Single or localized faults are generally referred to single bearing faults or tooth fault in gearboxes. This kind of failure generates an abnormal load affecting the machine torque. The global load torque can be modeled as a constant component Γ_0 and an fault component varying at the characteristic frequency f_d

$$\Gamma_{load}(t) = \Gamma_0 + \delta_\Gamma(t). \quad (1)$$

In this paper, the additional torque $\delta_\Gamma(t)$ is modeled as a periodic impulse signal with a periodicity related to the mechanical position (θ_m). The perturbance torque $\delta_\Gamma(t)$ is written using its Fourier serial as

* Corresponding author.
E-mail address: erik.etien@univ-poitiers.fr (E. Etien).

http://dx.doi.org/10.1016/j.measurement.2016.07.091
0263-2241/

$$\delta_\Gamma(t) = A \times R\left[1 + 2\sum_{n=1}^{\infty}\left(\frac{\sin(n\pi R)}{n\pi R}\cos(n\theta_d)\right)\right], \quad (2)$$

where A is the amplitude of the fault-related torque, R is the duty cycle defined by $R = \frac{\epsilon}{T_o}$ with ϵ the pulse width and T_o the related signal periodicity. The angle θ_d is related to the mechanical position θ_m by

$$\theta_d = N_i\theta_m. \quad (3)$$

The parameter N_i represents the number of impacts for one revolution. The following mechanical equation traduces the transfer of torque variations to the rotation speed signal.

$$w_m(t) = \frac{1}{J_m}\int_{t_0}^{t}(\Gamma_{motor}(\tau) - \Gamma_{load}(\tau))d\tau, \quad (4)$$

with J_m, the total inertia of the system.

Considering that the integration is a linear operation, then the rotational speed contains harmonics components at the same frequencies that (2). It can be used as an effective signal to perform fault detection. On the other hand, at variable speed, the fault frequencies are speed dependent. As a consequence, classical methods as Fourier analysis are difficult to applicate when signals are expressed as a function of time. In the following, we propose to express electrical and mechanical measurements (currents and speed) as a function of the mechanical position. It leads to spectra independent from speed variations.

3. Position synchronization for variable speed operations

At variable speed, the frequency analysis is complicated. To avoid this problem, electrical currents and mechanical speed are expressed as a function of the mechanical position. The position synchronization is presented in simulation on a PMSM controlled with a Field Oriented Control (Fig. 1). The PMSM model provides the mechanical speed (ω_m) which follows the reference ω_m^*. Mechanical position and speed are linked according to

$$w_m(t) = \frac{d}{dt}\theta_m(t) \quad (5)$$

The electrical position $\theta_e = p\theta_m$ (with p the number of pole pairs) is used to express currents and voltages in the park reference frame. The load torque $\Gamma_{load}(t)$ is considered as an input and defined by Eq. (1).

The synchronization signal $\theta_m(t)$ is provided by Eq. (5) knowing $w_m(t)$. From temporal signals $i(t)$, $\omega_m(t)$ and $\theta_m(t)$, synchronized signals $i(\theta_m)$, $\omega_m(\theta_m)$ are performed using an off-line interpolating procedure. In the following, a spectral analysis of signals $i(\theta_m)$, $\omega_m(\theta_m)$ will be used to detect faults signatures, then a constant position sampling Δ_θ period is sought. From the vector containing the mechanical position samples $\underline{\theta}_m = [\,\theta_m(0) \quad \theta_m(1) \quad \dots \quad \theta_m(N)\,]^T$ with N the number of samples, a new interpolated position vector is chosen as $\underline{\theta}^i_m = [\,\theta^i_m(0) \quad \theta^i_m(1) \quad \dots \quad \theta^i_m(N)\,]^T$. The constant sampling period is $\Delta\theta^i = \frac{\theta^i_m(N)-\theta^i_m(0)}{N}$ with $\theta^i_m(0) = \theta_m(0)$ and $\theta^i_m(N) = \theta_m(N)$. Considering this new vector, a linear 1-D data interpolation is performed on the current, the mechanical speed and the time samples:

$$\begin{aligned} t^i(\theta^i_m) &= \text{interp1}(\theta_m, t, \theta^i_m)\\ i^i(\theta^i_m) &= \text{interp1}(\theta_m, i, \theta^i_m)\\ \omega^i_m(\theta^i_m) &= \text{interp1}(\theta_m, \omega_m, \theta^i_m) \end{aligned} \quad (6)$$

After interpolation, a Fast Fourier Transform is applied on interpoled signals $i^i(\theta^i_m)$, $\omega^i_m(\theta^i_m)$:

$$\begin{aligned} I^i(k) &= \sum_{n=1}^{N} i^i(n)\exp\left(\frac{-2\pi j(k-1)(n-1)}{N}\right),\\ \Omega^i_m(k) &= \sum_{n=1}^{N}\omega^i_m(n)\exp\left(\frac{-2\pi j(k-1)(n-1)}{N}\right),\\ 1 <= k <= N \end{aligned} \quad (7)$$

Conventionally when the Fourier transform is applied to time dependent signals, the spectrum is expressed as a function of the frequency f in Hertz. To avoid any confusion, the spectrum obtained on signals varying as a function of the position is expressed in terms of a new variable g whose unit is the rad^{-1}. In Fig. 2, simulation results are shown for two speeds $\omega_{m1} = 78.5$ rad/s and $\omega_{m2} = 39.3$ rad/s (Fig. 2a). The sampling period is settled to $T_s = 10^{-4}$ s with a simulation duration $T = 10$ s. The PMSM nominal torque $\Gamma_0 = 7$ N m is applied at $t = 0.1$ s and added to the perturbance torque $\delta_\Gamma(t)$. The simulated fault is set at six impacts per turn (Fig. 2b).

Fig. 2c and d shows that the spectrum of the synchronized current and speed is independent of the motor operating point and is only linked to the number of impacts per revolution. Therefore, expressing the measurements according to the position, the spectral analysis is simplified. This analysis can be done on electric currents or speed. It is well known that information about the mechanical faults is very poor in the current amplitude. Many researches concern the use of currents instantaneous electrical frequency to perform mechanical diagnosis. For a PMSM, methods that use the instantaneous frequency to perform fault detection are equivalent to a mechanical speed analysis. Indeed, electrical frequency (f_e) is proportional to the mechanical speed according to

$$\omega_m = \frac{2\pi}{p}f_e \quad (8)$$

As a consequence, the mechanical speed is a very good candidate for fault detection. In the following, a soft sensor is designed to provide, in one hand the mechanical speed $\omega_m(t)$ containing fault signatures and on the other hand the angle $\theta_m(t)$ allowing the synchronization of motor measurements.

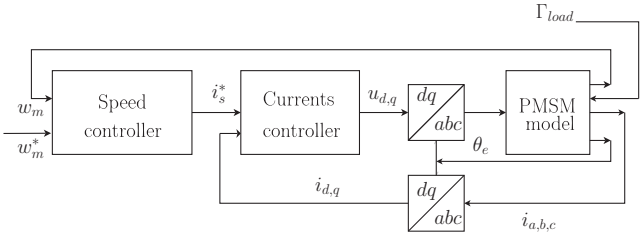

Fig. 1. PMSM Field Oriented Control.

4. Soft sensor design for speed measurement

In Section 2, it has been shown that the rotational speed is an effective signal to perform fault detection. Furthermore, we have shown that synchronizing the measurements with the shaft position, the spectral representation became independent of the rotational speed. In practical applications, speed and position measurements can be expensive and difficult to implement. Then, a soft sensor providing both these two signals is an interesting alternative. However, harmonic amplitudes can be small and difficult to detect. Results depend on mechanical characteristics, in particular the total inertia J_m. Then, it is interesting to use a speed signal where fault frequencies could be amplified. Here, this goal was achieved by the use of an appropriate design of the soft sensor.

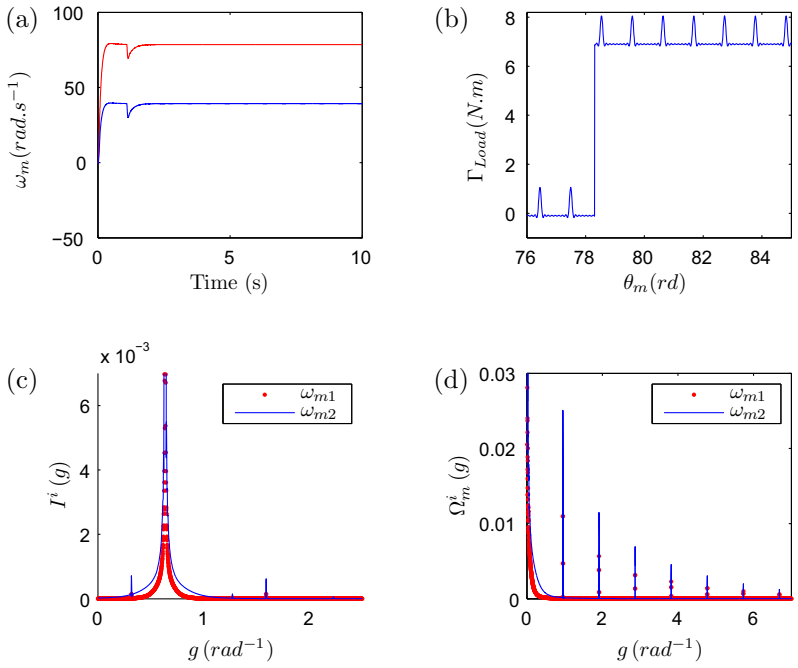

Fig. 2. Synchronization.

4.1. Soft sensor model

The soft sensor proposed in this section is based on an adaptive observer [20]. Rotor speed and position estimations use information contained in the error between the measured stator currents and the estimated ones. An adaptation mechanism is built using the stator currents error estimation in order to estimate the rotor speed. The adjustable model is fed back by the output of the adaptation mechanism, i.e. the rotor speed in the present case. The adaptive observer scheme is represented in Fig. 3, where stator currents are chosen as state variables in the adjustable model.

The adaptive observer model can be written as (superscript $\widehat{\cdot}$ denotes the estimated quantities)

$$\dot{\widehat{\psi}}_s = u_s - R_s\widehat{i}_s - p\widehat{\omega}_m J\widehat{\psi}_s + \lambda\tilde{i}_s, \tag{9}$$

where $u_s = [u_d \quad u_q]^T$ is the stator voltage vector, $\widehat{i}_s = \left[\widehat{i}_d \quad \widehat{i}_q\right]^T$ is the estimated stator current vector, $\widehat{\psi}_s = \left[\widehat{\psi}_d \quad \widehat{\psi}_q\right]^T$ is the estimated stator flux linkage, R_s is the stator resistance, $\widehat{\omega}_m = \dot{\widehat{\theta}}_m$ is the estimated angular speed of the rotor. J is a square matrix represented as

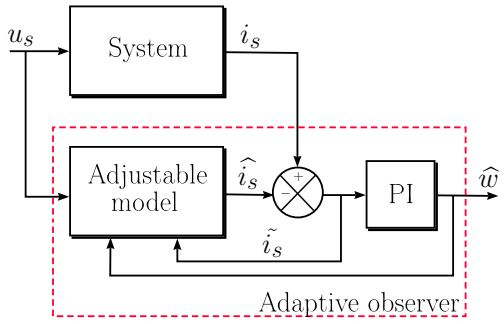

Fig. 3. Block diagram of the system and the adaptive observer.

$$J = \begin{bmatrix} 0 & -1 \\ 1 & 0 \end{bmatrix}$$

The stator currents estimation and its error are respectively defined as

$$\tilde{i}_s = i_s - \widehat{i}_s. \tag{10}$$

The flux equation id defined by

$$\widehat{i}_s = L^{-1}\left(\widehat{\psi}_s - \psi_{pm}\right), \tag{11}$$

where ψ_{pm} is the permanent magnet flux expressed as $\psi_{pm} = [\psi_{pm} \quad 0]^T$ and L is the inductance matrix which depends respectively on the direct and quadrature axis inductances L_d and L_q:

$$L = \begin{bmatrix} L_d & 0 \\ 0 & L_q \end{bmatrix} \tag{12}$$

λ is the feedback gain matrix. In order to place two poles of the observer in the complex plane at a specific location, λ should include a symmetric part and skew symmetric part as it is expressed in (13), where I represents the two by two identity matrix and λ_1, λ_2 are scalar gain parameters.

$$\lambda = \lambda_1 I + \lambda_2 J \tag{13}$$

There are several alternative ways to calculate the currents error. In the following, the error is calculated as

$$\epsilon = [0 \quad L_q] \cdot \tilde{i}_s \tag{14}$$

To estimate the electrical angular speed of the rotor, an adaptation mechanism based on Proportional-Integral (PI) regulator is used.

$$\widehat{\omega} = p\widehat{\omega}_m = -k_p \cdot \epsilon - k_i \int \epsilon \cdot dt \tag{15}$$

where k_p and k_i are coefficients of the PI regulator. The estimated rotor position $\widehat{\theta}_m(t)$ is obtained by integrating the estimated rotor

angular speed $\widehat{\omega}_m(t)$. In the following, estimations are used to provide both the speed $\widehat{\omega}_m(t)$ containing fault information and the mechanical position $\widehat{\theta}_m(t)$ allowing the synchronization procedure.

4.2. Soft sensor design

The soft sensor is designed using the four parameters λ_1, λ_2, k_p and k_i. Feedback gains λ_1 and λ_2 affect the currents observation dynamics, while k_p and k_i affect the dynamic of the estimated speed. In order to simplify the design, a linearization at an operating point of the observer model (9) is performed using the adaptation law (15) as an additional state. According to the system linearization method mentioned in [19], the state vector x can be written as

$$x = x_0 + \delta x \tag{16}$$

where $x_0 = [\,id_0 \quad iq_0 \quad w_0\,]$ and $\delta x = [\,\delta id \quad \delta iq \quad \delta w\,]$. Expressing the resulting system in a component form, the linearized model is defined as

$$\frac{d}{dt}\begin{bmatrix}\delta\widehat{id}\\ \delta\widehat{iq}\\ \delta\widehat{w}\end{bmatrix} = [A]\begin{bmatrix}\delta\widehat{id}\\ \delta\widehat{iq}\\ \delta\widehat{w}\end{bmatrix} + [B]\begin{bmatrix}\delta vd\\ \delta vq\\ \delta id\\ \delta iq\\ \delta w\end{bmatrix} \tag{17}$$

$$y = [C]\begin{bmatrix}\delta\widehat{id}\\ \delta\widehat{iq}\\ \delta\widehat{w}\end{bmatrix} \tag{18}$$

where

$$A = \begin{bmatrix} \frac{-R_s}{L_d} - \lambda_1 & \frac{L_q}{L_d}w_0 + \lambda_2 & \frac{L_q}{L_d}iq_0 \\ \frac{-L_d}{L_q}w_0 - \lambda_2 & \frac{-R_s}{L_q} - \lambda_1 & \frac{\psi_{pm}}{L_q} - \frac{L_d}{L_q}id_0 \\ -a_1 & -a_2 & -a_3 \end{bmatrix}$$

$$B = \begin{bmatrix} \frac{1}{L_d} & 0 & \lambda_1 & -\lambda_2 & 0 \\ 0 & \frac{1}{L_q} & \lambda_2 & \lambda_1 & 0 \\ 0 & 0 & a_1 & a_2 & a_3 \end{bmatrix}$$

$$C = \begin{bmatrix} 1 & 0 & 0 \\ 0 & 1 & 0 \\ 0 & 0 & 1 \end{bmatrix}$$

The subscript 0 stands for the operating point quantities. Parameters b_0, b_1, b_2 and b_3 are given in the appendix at the end of this paper. The stator currents and the angular speed become new inputs of the linearized system. Estimated current and speed are the outputs.

4.2.1. Design of matrix λ

A judicious choice of λ_1 gives to the soft sensor fast dynamics compared to the FOC current loop one. The state matrix A is defined as

$$A = \begin{bmatrix} \frac{-R_s}{L_d} - \lambda_1 & \frac{L_q}{L_d}w_0 + \lambda_2 & \frac{L_q}{L_d}iq_0 \\ \frac{-L_d}{L_q}w_0 - \lambda_2 & \frac{-R_s}{L_q} - \lambda_1 & \frac{\psi_{pm}}{L_q} - \frac{L_d}{L_q}id_0 \\ -a_1 & -a_2 & -a_3 \end{bmatrix}$$

Eigen values of the model (17) and (18) can be calculated solving: $det[sI - (A - \lambda C)] = 0$. Fig. 4 shows in the $\Re/Im$ plane the observer and the FOC eigen values respectively for $\lambda_1 = 5$ and $\lambda_2 = 0$. It can be noticed that for this value of λ_1, the observer dynamics is faster than the FOC currents dynamics.

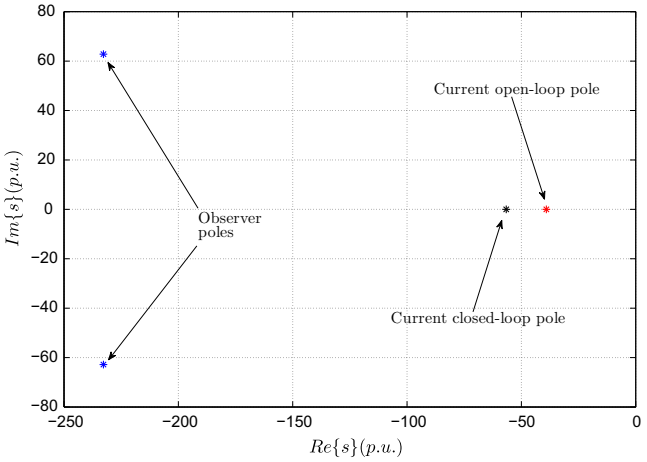

Fig. 4. Current open-loop, current closed-loop and observer poles for $\lambda_1 = 5$.

4.2.2. Design of PI parameters k_p and k_i

PI parameters k_p and k_i allow to adjust the dynamic of the estimated speed. The transfer function between the measured and estimated variables is given by

$$F = C(sI - A)^{-1}B = \begin{bmatrix} F_{11} & F_{12} & \cdots & F_{15} \\ F_{21} & F_{21} & \cdots & F_{25} \\ F_{31} & F_{32} & \cdots & F_{35} \end{bmatrix} \tag{19}$$

The transfer function $F_{34}(s) = \frac{\widehat{\omega}_m(s)}{iq(s)}$ is particularly interesting. Indeed, its input is the current i_q which is proportional to the motor torque when it is driven with a FOC. In steady state i_q is directly linked to the load torque containing all the information about the fault. The transfer function between the stator current iq and the estimated speed $\widehat{w}$ is written as

$$F_{34}(s) = \frac{\widehat{w}(s)}{i_q(s)} = \frac{a_{34.2}s^2 + a_{34.1}s + a_{34.0}}{b_3s^3 + b_2s^2 + b_1s + b_0} \tag{20}$$

The denominator parameters b_0, b_1, b_2 and b_3 are given in Appendix A. It depend on the operating point w_0, iq_0, id_0 and of the three parameters k_i, k_p, λ_1 and λ_2. In order to simplify this transfer function, λ_2 and id_0 are fixed to 0. Thus, for a specified operating point, the resulting transfer function can be written as

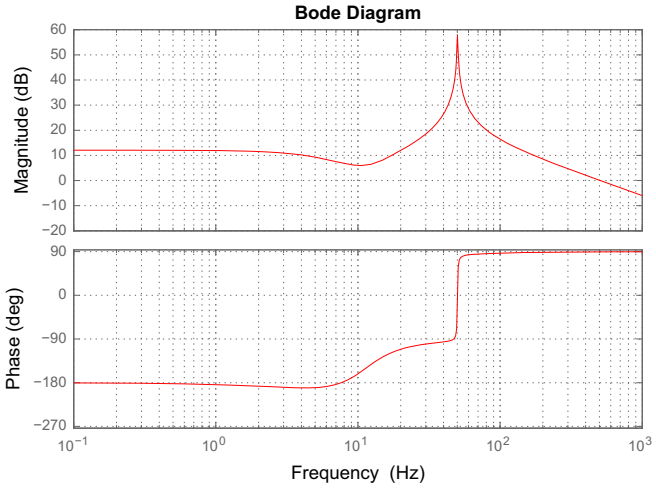

Fig. 5. Bode diagram of the function $F_{34}(s)$ for $\lambda_1 = 15$, $\lambda_2 = 0$, $k_i = 100$ and $k_p = 0.05$.

a filter where k_i, k_p and λ_1 are setting parameters. The Bode diagram of the function $F_{34}(s)$ is given in Fig. 5 for $\lambda_1 = 15$, $\lambda_2 = 0$, $k_i = 100$ and $k_p = 0.05$, $w_0 = 62.83$ rad/s and $iq_0 = 1.78$ A. According to this figure, we can see that the frequency response of the function $F_{34}(s)$ corresponds to a low-pass filter with a resonance frequency. This resonance frequency can be used for fault detection to amplify the fault signatures in frequency domain by adjusting the three parameters k_i, k_p and λ_1 to make coincide the fault frequency with the resonance frequency. The complete study of parameters influence on frequency response is not presented in this paper but will be discussed in the conclusion.

5. Experimental results

Figs. 6 and 7 illustrate the complete experimental setup which includes two Permanent Magnet Synchronous Machines. The synchronous motor (PMSM) is driven by a variable-speed drive (VSD). The rotor position (measured by an incremental encoder) is returned directly to the VSD. The Permanent Magnet Synchronous Generator (PMSG) is connected to a passive load. The signals recording is performed by a dSPACE-DS1104 card and the acquisition is made in MATLAB environment. The localized fault is emulated using an original mechanical system designed in our laboratory. The emulator is mounted on the coupling motor/generator. It consists of a roller mounted vertically over a 9 teeth sprocket. This system emulates a fault occurring 9 times per turn. A spring is mounted above the roller to adjust the force in order to get different fault severities.

According to (6), the data interpolation is now performed with the estimated signals $\widehat{\omega}_m(t)$ and $\widehat{\theta}_m(t)$.

$$\widehat{\omega}^i_m(\widehat{\theta}^i_m) = \text{interp1}(\widehat{\theta}_m, \widehat{\omega}_m, \widehat{\theta}^i_m) \tag{21}$$

The estimated position $\widehat{\theta}_m(t)$ is also used to calculate the observer currents $(\widehat{i}_d, \widehat{i}_q)$ in the park reference frame.

The PMSM is driven around the mean speed $\widehat{\omega}_{mo} = 16$ rad/s with a constant load torque T_{Lo}. The spectrum of the synchronized estimated speed is shown in Fig. 8b. A component at $g_1 = \frac{p}{2\pi}$ is highlighted (with p the PMSM number of poles pairs). In the soft sensor, the estimated speed is simulated using currents and voltages, then components linked to electrical frequency subsist. In Fig. 9, amplitude components are zoomed around characteristic components. Let us define $g_d = \frac{9}{2\pi}$, the fundamental component corresponding to the emulated fault (nine impacts per revolution). We can see that g_d and its harmonics are present in the spectrum of the synchronized estimated speed. The synchronization with the estimated position leads to an equivalent spectrum independent from speed variations.

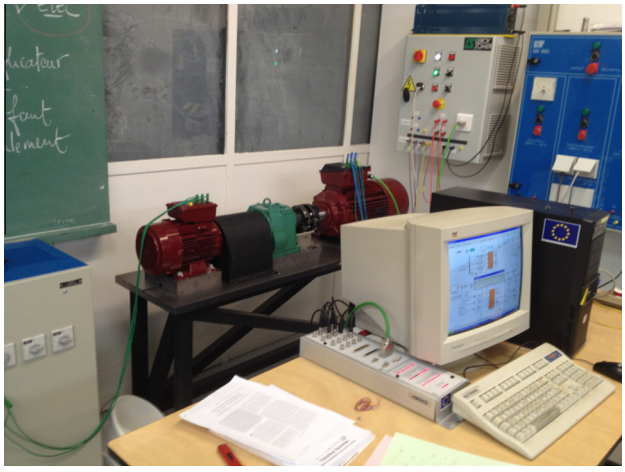

Fig. 6. Experimental setup.

Fig. 7. Localized fault emulator.

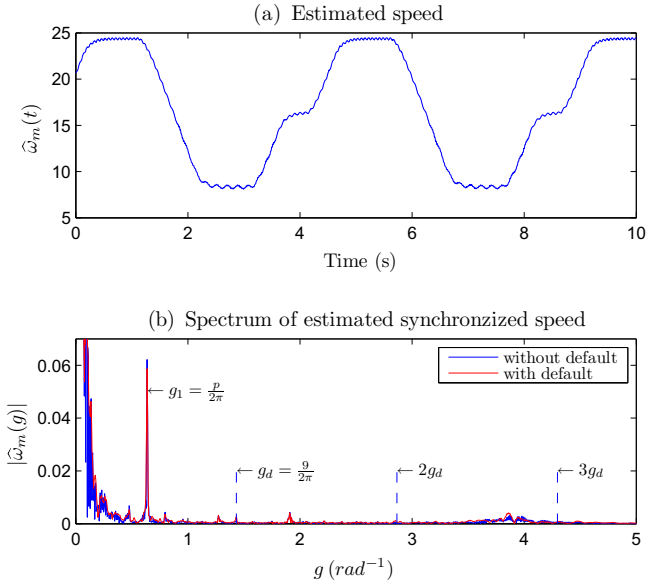

Fig. 8. Spectrum of synchronized estimated speed.

In order to detect the emulated fault, an energy indicator is used. First, the components related to impacts are isolated using a Time Synchronous Averaging (TSA) method [24]. The following filter is defined:

$$\text{TSA}(g) = \left| \frac{\sin(\pi N T_d f)}{N \sin(\pi N T_d f)} \right| \tag{22}$$

with $T_d = \frac{1}{g_d} = \frac{2\pi}{9}$ and $N = 50$. Samples calculated with the Fourier transform are simply multiplied term by term with those calculated by (22). The resulting spectrum is shown in Fig. 10a. In a second step, a band pass filter (BPF) is applied to select a band in which the energy criterion will be calculated. We choose to only consider the four first components from g_d to $4g_d$ (Fig. 10b).

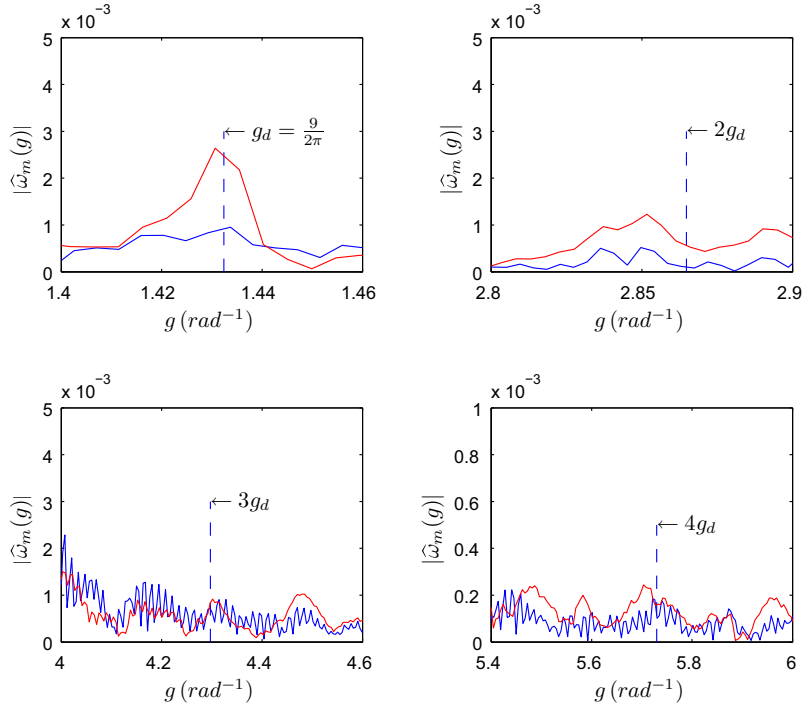

Fig. 9. Spectrum of synchronized estimated speed (zoom). Without fault (blue), with fault (red). (For interpretation of the references to color in this figure legend, the reader is referred to the web version of this article.)

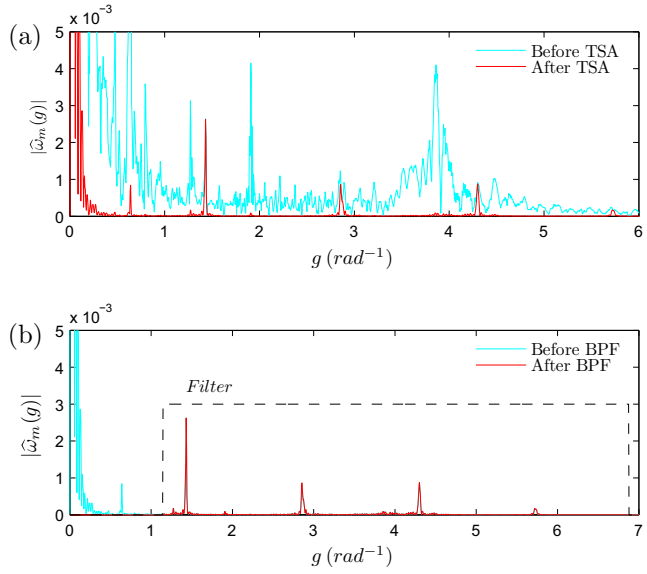

Fig. 10. Spectrum of synchronized estimated speed. (a) TSA filtering, (b) BP filtering.

Table 1
Spectral energy indicator.

Test conditions	IND
Healthy	$6,2 \cdot 10^{-6}$
Fault	$2,15 \cdot 10^{-5}$

The following indicator is calculated from the filtered signal:

$$I = \underline{X}^T \cdot \underline{X} \tag{23}$$

with $\underline{X}$ the vector containing samples of the filtered signal. The indicator I is homogeneous to the energy spectrum of the filtered signal. Finally, the proposed method is applied to two tests without and with fault, and results are shown in Table 1.

The variation of the indicator based on spectral energy is, in this case, sufficient to detect the fault. The complete procedure is experimentally validated on this example.

6. Conclusion

This paper presents a procedure using a speed soft sensor for the detection of mechanical faults in electrical drives. The soft sensor provides both the speed which contains fault information and the position which allows to synchronize measurements in order to become speed independent. This solution is very interesting for applications where no mechanical sensor is available. In future works, the soft sensor design will be developed. It has been shown that a resonance can be obtained with an appropriate choice of PI parameters. In fact, it can be demonstrated that only k_i influences the resonance frequency. However, at variable speed this parameter might be adapted as a function of the actual speed leading to a Linear Parameter-varying controller. Amplification using the soft sensor model is crucial to ensure that the fault can be detected specially when its amplitude is small compared to the motor load torque or if measurements are very noisy.

Appendix A

$$
\begin{cases}
b_3 = L_d^2 L_q^3 \\
b_2 = L_d L_q (k_p L_d^2 L_q i d_0^2 + k_p L_d^2 i d_0 \phi_f + 2\lambda_1 L_d L_q^2 \\
\quad + k_p L_d L_q i d_0 \phi_f + R_s L_d L_q + k_p L_d \phi_f^2 + k_p L_q^3 i q_0^2 \\
\quad + RsL_q^2) \\
b_1 = L_d Lq (k_p L_d^2 L_q i d0^2 \lambda_1 + k_i L_d^2 L_q i d_0^2 - k_p L_d^2 L_q i d_0 i q_0 \lambda_2 \\
\quad + L_d^2 L_q \lambda_2 w_0 + k_p L_d^2 i d_0 \lambda_1 \phi_f + k_i L_d^2 i d_0 \phi_f + L_d L_q^2 \lambda_1^2 \\
\quad + LdLq^2 \lambda_2^2 + L_d L_q^2 w_0^2 + k_p L_d L_q R_s i d_0^2 + L_d L_q R_s \lambda_1 \\
\quad + k_p L_d L_q i d_0 \lambda_1 \phi_f + k_i L_d L_q i d_0 \phi_f - k_p L_d L_q i q_0 \lambda_2 \phi_f \\
\quad + k_p L_d L_q i q_0 \phi_f w_0 + k_p L_d R_s i d_0 \phi_f + k_p L_d \lambda_1 \phi_f^2 \\
\quad + k_i L_d \phi_f^2 + k_p L_q^3 i d_0 i q_0 \lambda_2 + k_p L_q^3 i q_0^2 \lambda_1 + k_i L_q^3 i q_0^2 \\
\quad + L_q^3 \lambda_2 w_0 + k_p L_q^2 R_s i q_0^2 + L_q^2 R_s \lambda_1 + k_p L_q^2 i q_0 \lambda 2 \phi_f \\
\quad - k_p L_q^2 i q_0 \phi_f w_0 + L_q R_s^2 + kpL_q R_s i d_0 \phi_f + k_p R_s \phi_f^2) \\
b_0 = L_d L_q (R_s k_i \phi_f^2 + L_d k_i \lambda_1 \phi_f^2 + L_q^2 R_s i q_0^2 k_i + L_q^3 i q_0^2 k_i \lambda_1 \\
\quad + L_d R_s i d_0 k_i \phi_f + L_q R_s i d_0 k_i \phi_f + L_d L_q R_s i d_0^2 k_i \\
\quad + L_q^3 i d_0 i q_0 k_i \lambda_2 + L_d^2 i d_0 k_i \lambda_1 \phi_f + L_q^2 i q_0 k_i \lambda_2 \phi_f \\
\quad - L_q^2 i q_0 k_i \phi_f w_0 + L_d^2 L_q i d_0^2 k_i \lambda_1 - L_d^2 L_q i d_0 i q_0 k_i \lambda_2 \\
\quad + L_d L_q i d_0 k_i \lambda_1 \phi_f - L_d L_q i q_0 k_i \lambda_2 \phi_f + L_d L_q i q_0 k_i \phi_f w_0)
\end{cases}
$$

References

[1] H. Cao, F. Fein, K. Zhou, Z. He, Wheel-bearing fault diagnosis of trains using empirical wavelet transform, Measurement 82 (2016) 439–449.

[2] J. Xiang, Y. Zhong, H. Gao, Rolling element bearing fault detection using PPCA and spectral kurtosis, Measurement 75 (2015) 180–191.

[3] X. Zhang, Y. Liang, J. Zhou, Y. Zang, A novel bearing fault diagnosis model integrated permutation entropy, ensemble empirical mode decomposition and optimized SVM, Measurement 69 (2015) 164–179.

[4] F. Chen, B. Tang, R. Chen, A novel fault diagnosis model for gearbox based on wavelet support vector machine with immune genetic algorithm, Measurement 46 (2013) 220–232.

[5] J. Mei, Y. Xiao, X. Chen, L. Qiao, Fault diagnosis of a gearbox based on the analysis of a fractional energy gathering band, Measurement 46 (2013) 3662–3670.

[6] C. Hu, W.A. Smith, R.B. Randall, Z. Peng, Development of a gear vibration indicator and its application in gear wear monitoring, Mech. Syst. Signal Process. (2016). Available online 10 February.

[7] V.F. Pires, M. Kadivonga, J.F. Martins, A.J. Pires, Motor square current signature analysis for induction motor rotor diagnosis, Measurement 46 (2013) 942–948.

[8] E.H. El Bouchikhi, V. Choqueuse, M.E.H. Benbouzid, Induction machine faults detection using stator current parametric spectral estimation, Mech. Syst. Signal Process. 52–53 (2014) 447–464.

[9] F. Gu, T. Wang, A. Alwodai, X. Tian, Y. Shao, A.D. Ball, A new method of accurate broken rotor bar diagnosis based on modulation signal bispectrum analysis of motor current signals, Mech. Syst. Signal Process. 50–51 (2015) 400–413.

[10] B. Trajin, J. Regnier, J. Faucher, Comparison between stator current and estimated mechanical speed for the detection of bearing wear in asynchronous drives, IEEE Trans. Ind. Electron. 56 (11) (2009) 4700–4709.

[11] V.F. Pires, M. Kadivonga, J.F. Martins, A.J. Pires, Estimating and interpreting the instantaneous frequency of a signal. I. Fundamentals, Proc. IEEE 80 (4) (1992) 520–538.

[12] A. Lebaroud, G. Clerc, Diagnosis of induction motor faults using instantaneous frequency signature analysis, in: 18th International Conference on Electrical Machines (ICEM), Vilamoura, Portugal, 2008, pp. 1–5.

[13] M. Pineda-Sanchez, M. Riera-Guasp, J. Pons-Llinares, V. Climente-Alarcon, J. Perez-Cruz, Diagnosis of induction machines under transient conditions through the Instantaneous Frequency of the fault components, in: XIX International Conference on Electrical Machines (ICEM), Rome, Italy, 2010, pp. 1–6.

[14] M. Hamadache, D. Lee, K.C. Veluvolu, Rotor speed-based bearing fault diagnosis (RSB-BFD) under variable speed and constant load, IEEE Trans. Ind. Electron. (99) (2015).

[15] T. Wang, M. Liang, J. Li, W. Cheng, C. Li, Bearing fault diagnosis under unknown variable speed via gear noise cancellation and rotational order sideband identification, Mech. Syst. Signal Process. 62–63 (2015) 30–53.

[16] C. Mishra, A.K. Samantaray, G. Chakraborty, Rolling element bearing defect diagnosis under variable speed operation through angle synchronous averaging of wavelet, Mech. Syst. Signal Process. 72–73 (2016) 206–222.

[17] J. Shi, M. Liang, Y. Guan, Bearing fault diagnosis under variable rotational speed via the joint application of windowed fractal dimension transform and generalized demodulation: a method free from prefiltering and resampling, Mech. Syst. Signal Process. 68–69 (2016) 15–33.

[18] L.F. Villa, A. Renones, J.R. Pera, L.J. de Miguel, Angular resampling for vibration analysis in wind turbines under non-linear speed fluctuation, Mech. Syst. Signal Process. 25 (2011) 2157–2168.

[19] E. Etien, Modeling and simulation of soft sensor design for real-time speed estimation, measurement and control of induction motor, ISA Trans. 55 (3) (2013) 358–364.

[20] I. Omrane, E. Etien, W. Dib, O. Bachelier, Modeling and simulation of soft sensor design for real-time speed and position estimation of PMSM, ISA Trans. 57 (2015) 329–339.

[21] B. Trajin, J. Regnier, J. Faucher, Detection of bearing faults in asynchronous motors using Luenberger speed observer, in: 34th Annual Conference of the IEEE Industrial Electronics Society (IECON), Vienna, Austria, Orlando, USA, 2008, pp. 3073–3078.

[22] A. Piippo, M. Hinkkanen, J. Luomi, Analysis of an adaptive observer for sensorless control of interior permanent magnet synchronous motors, IEEE Trans. Ind. Electron. 55 (3) (2008) 570–576.

[23] E. Etien, C. Chaigne, N. Bensiali, On the stability of full adaptive observer for induction motor in regenerating mode, IEEE Trans. Ind. Electron. 57 (5) (2010) 1599–1608.

[24] M.L. Masmoudi, E. Etien, S. Moreau, A. Sakout, Bearing fault diagnosis using a pre-filtering and a spectral identification algorithm, in: 39th Annual Conference of the IEEE Industrial Electronics Society (IECON), Vienna, Austria, 2013, pp. 5476–5481.